Source Process of very long period seismic events associated with the 1998 activity of Iwate Volcano, northeastern Japan

doi: 10.1029/2000JB900155

JOURNAL OF GEOPHYSICAL RESEARCH, VOL. 105, NO. B8, PAGES 19,135-19,147, AUGUST 10, 2000

Source process of very long period seismic events associated with the 1998 activity of Iwate Volcano, northeastern Japan

Takeshi Nishimura, [1,2] Haruhisa Nakamichi,[2] Satoru Tanaka, [2] Minemori Sato, [2]
Tomokatsu Kobayashi, [1] Sadato Ueki, [2] Hiroyuki Hamaguchi, [2]
Masakazu Ohtake, [1] and Haruo Sato[1]

Abstract. We observed very long period seismic events that are associated with the 1998 activity of Iwate Volcano, northeast Japan. The events show a dominant period of 10 s and duration of 30-60 s, often with accompanying short-period waves at the beginning and at the end of the long-period signals. By analyzing the broadband seismograms we find that the source elongates in the east-west direction for ~ 4 km at a depth of 2 km beneath the western part of Iwate Volcano. Results of moment tensor inversions show a source mechanism of mutual deflation and inflation of two chambers located at the western and eastern edges of the source region. The source region coincides with the low seismic velocity zone detected by seismic tomography and is very close to the locations of pressure sources estimated from crustal deformation data. On the basis of these results we infer that the very long period seismic events are generated by transportation and movement of magmatic fluid (hot water and/or magma) in a shallow part of the volcano. We further present a simple source model of very long period seismic events based on one-dimensional flow dynamics and propose a new parameter to characterize the size of very long period event: the energy flow rate, which is obtained by dividing the seismic moment by the dominant period. The energy flow rate was estimated as 3.1 x 10^{12} J/s for the event on July 29, 1998.

1. Introduction

Mount Iwate group is located in the northern part of Honshu, Japan (Figure 1). The volcanic group consists of the western part (hereafter referred to as Nishi-Iwate) and the eastern part (referred to as Higashi-Iwate). The activity of Nishi-Iwate started ~300 kyr ago; Higashi-Iwate was formed ~30 kyr ago [*Doi*, 1999; *Nakagawa*, 1987; *Nakagawa and Togari*, 1999]. Volcanic activities of Nishi-Iwate are characterized mainly by phreatic eruptions. The latest phreatic eruption occurred inside the Onigajo caldera in 1919. On the other hand, Higashi-Iwate has repeatedly experienced both phreatic and magmatic eruptions. In 1686-1687 a significant eruption accompanying volcanic explosions, scoria effusions, volcanic lahars, and pyrocrastic surges occurred at the summit of Higashi-Iwate. In 1732, basaltic lava effused from several vents newly formed on the eastern flank of Higashi-Iwate and the lava flow reached as far as ~3 km (Yakebashiri lava flow). In 1990s, strong fumerol activities and steam explosions were sometimes observed near the summit of Higashi-Iwate.

A volcanic tremor was first detected in September 1995 after construction of a seismic station close to Iwate Volcano in 1981 [*Ueki et al.*, 1996]. It was ~10 months after the Far-East off Sanriku earthquake (M_w7.7) located ~100 km east of the volcano on December 28, 1994 [*Nakahara et al.*, 1998; *Nishimura et al.*, 1996]. Since then (September 1995), volcanotectonic earthquakes (which are caused by a faulting) and low-frequency events have been observed mainly at Higashi-Iwate. Although the activity was not so significant, the number of earthquakes gradually increased from the end of December 1997 [*Tanaka et al.*, 1999a]. In February 1998, crustal deformations were detected by three borehole strain meters installed around the volcano, and in the middle of March, strong swarms of the volcanotectonic events and low-frequency seismic events occurred in a shallow part of Nishi-Iwate. Such volcanic activities continued at a high level for 5 months from April to August 1998. In June the Japan Meteorological Agency (JMA) publicly announced a possibility of an eruption of the volcano. On September 3, 1998, an *M*6.1 earthquake took place near the south flank of Nishi-Iwate [*Nakahara et al.*, 1999]. After the earthquake occurrence, the number of volcanic earthquakes around Nishi-Iwate decreased, and crustal deformation changes became smaller. However, seismic activity and crustal deformation still continue at a higher level compared with those before 1998, although no significant eruptions have yet been reported (February 2000).

To detect seismic signals associated with the activity of Iwate Volcano, we started a broadband seismic observation at Genbudo station (GNB) on the southern flank of Nishi-Iwate on April 2, 1998 (see Figure 1). At this site we detected a large number of very long period seismic events having a dominant period of 10 s. This was the first time such long-period seismic signals originating from Iwate Volcano were detected. Figure 2 shows an example of a swarm of the very long period events. Similar events have been recently reported at several volcanoes, such as Stromboli in Italy [*Neuberg et al.*, 1994], Aso in Kyushu, Japan [*Kaneshima et al.*, 1996],

[1]Department of Geophysics, Graduate School of Science, Tohoku University, Sendai, Japan.
[2]Research Center for Prediction of Earthquakes and Volcanic Eruptions, Graduate School of Science,
Tohoku University, Sendai, Japan.

Paper number 2000JB900155.
0148-0227/00/2000JB900155$09.00

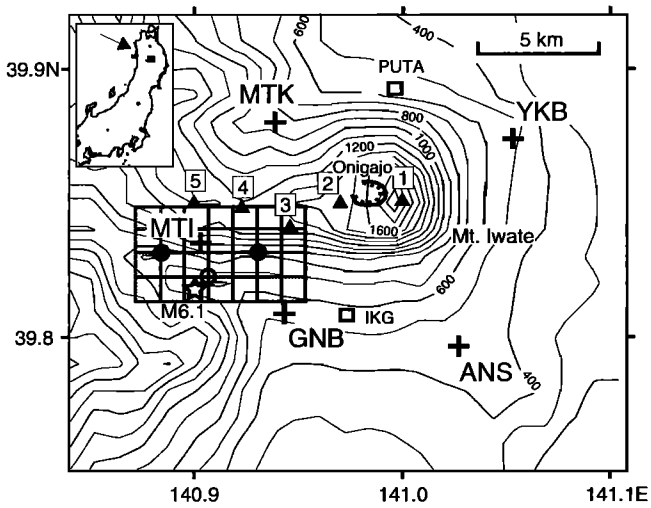

Figure 1. Location map of the broadband seismic stations (pluses). Numbered solid triangles represent peaks of Iwate Volcano (1, Yakushi-dake; 2, Kurokura-yama; 3, Inukura-yama; 4, Ohmatsukura-yama; 5, Mitsuishi-yama). Peak 1 (the summit of Iwate Volcano) is located in the Higashi-Iwate (the eastern part of the volcano), and the other peaks (2-5) belong to the Nishi-Iwate (the western part). Epicenter of the *M*6.1 earthquake on September 3, 1998, is shown by a star. Grid points of the gray lines are used for candidates of point sources of very long period seismic evnets. The location of the best two point sources and that of one point source estimated from moment tensor inversion are represented by solid and open circles, respectively (see text for details). PUTA and IKG (open squares) are Global Positioning System stations. Seismic station HSB is off Figure 1.

and Erebus in the Antarctica [*Rowe et al.*, 1998]. These very long period events are often observed at very active volcanoes; hence the events are considered to be closely related to the magma and/or hot water activity in a shallow part of the volcano [e.g., *Kaneshima et al.*, 1996]. Since, compared with high-frequency waves, the seismic waves of very long period events are less distorted by complex structures of the volcano, it is possible to determine accurately the source mechanisms if a dense seismic observation is available. For this reason many seismologists and volcanologists have used investigations of the very long period events as a tool to understand the dynamics of volcanoes [*Kaneshima et al.*, 1996; *Neuberg et al.*, 1994; *Ohminato et al.*, 1998, *Rowe et al.*, 1998].

In this study, we analyze in detail the very long period seismic events (hereafter referred to as VLPs) observed at Iwate Volcano. We first investigate waveform characteristics of VLPs and determine the hypocenter from particle orbit and semblance analyses. Next, we apply a waveform inversion technique to estimate moment tensor time functions of the VLP source. Finally, we propose a source mechanism of VLP taking into consideration the results of other geophysical observations, such as microearthquake activity, crustal deformation, and volcano structure to clarify underground process of the 1998 activity of Iwate Volcano.

2. Observation

After the installation of a broadband seismometer at GNB on April 2, 1998, we deployed five additional stations around Iwate Volcano (Ainosawa station (ANS) was started on April 13; Yakebashiri (YKB) was started on April 13; Hashiba (HSB) was started on June 13; Mitsuishi (MTI) was started on July 14; and Matsukawa (MTK) was started on July 25) by the end of July, 1998. The station locations are shown in Figure 1. The same type of broadband three-component seismometer (STS-2; Streckeisen) is installed at each of the six stations. The seismometers at MTI and MTK are set on a flat concrete base on the ground surface and are surrounded by concrete blocks to prevent temperature changes and effects of the wind. Seismometers at other stations are fixed on the concrete base of the buildings of permanent seismic stations of the Research Center for Prediction of Earthquakes and Volcanic Eruptions (RCPEV), Tohoku University. Output signals of the broadband seismometer at each station are continuously recorded by a digital data recorder (LS8000WD, Hakusan Co.) with an analog to digital (A/D) resolution of 24 bits and a sampling interval of 0.02 s. The internal crystal clock of the recorder (precision better than 10^{-6}) is corrected every 2 hours by Global Positioning System (GPS) time signals, so that the error in the recorded time is < 8 ms.

At the GNB station we have also observed volumetric strain and ground tilt since the end of October 1997. A borehole tilt meter [*Sato et al.*, 1980] and a strain meter [*Sacks et al.*, 1971] are embedded at a depth of 300 m from the ground surface. Their signals are digitized with an A/D resolution of 22 bits and a sampling interval of 1 s and are continuously transmitted to RCPEV through a telephone line.

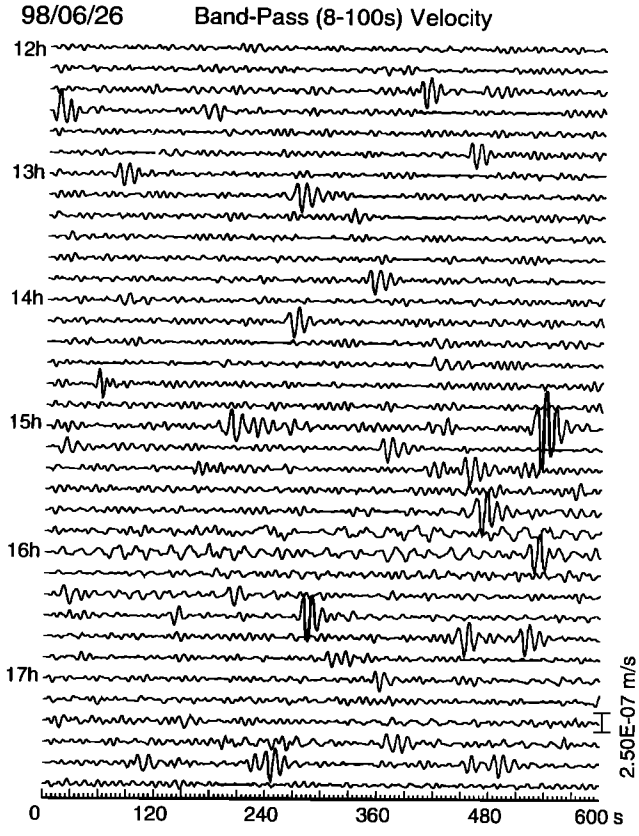

Figure 2. An example of the very long period seismic signals observed at GNB station on June 26, 1998. The vertical component of broadband seismogram is band-pass filtered for a period from 8 to 100 s. Read 98/06/26 as June 26, 1998.

These data are also used in the present study. Strain and tilt observations are also carried out at stations ANS and YKB, but the sampling interval is 1 min, so we do not use those data in this study.

3. Characteristics of Very Long Period Seismic Events

Figure 3a shows the cumulative number of VLPs observed at GNB. We read the occurrence time of VLP from the borehole strain data instead of the seismograms, since the strain records are available from the end of November 1997. To avoid miscount of other seismic events, we carefully checked origin times of local and regional earthquakes by using the database of JMA. Activity of VLPs was very high for the period from April to August, especially in the middle of April and from the end of June to the beginning of July. However, after the occurrence of the *M*6.1 earthquakes on September 3, 1998, VLP activity decreased dramatically.

Figure 4a shows displacement seismograms of vertical components of VLP recorded by a STS-2 installed at GNB station. Most of the VLPs have a dominant period of 10 s and signal duration of 30–60 s. These characteristics of the waveforms are common for all VLP events observed for the period from April to August 1998, which implies that each of VLP is excited by a similar process (but not the same). Most of the events show downward initial motions, although there are a few events having upward initial motions (e.g., events on June 28, 1998, 2230 LT and August 22, 1998, 2230 LT). Figure 4b shows examples of 1-10 Hz band-pass filtered velocity seismograms for the same events in Figure 4a. It is found that the VLPs are often accompanied by high-frequency signals at the beginning and/or at the end of long-period (10 s) signals. Because of unclear onsets of the signals we could not determine the hypocenter of high-frequency signals by using first arrival times. In Figure 5 an example of the velocity spectrum of VLP is plotted. The dominant peak of the spectrum is at 0.1 Hz (10 s in period). A second one is recognized around 0.2 Hz (5 s), which nearly coincides with a half period of the first peak. Figure 5 indicates that the VLP event has a wide spectrum from 0.02 to 10 Hz. Signal spectrum between 0.3 and 1 Hz is masked by noises mainly caused by oceanic waves, but seismic signals of the VLP are still recognized for high frequencies beyond 1 Hz. However, we do not investigate further the characteristics of the waves at high frequency (>0.2 Hz) owing to lack of good signal to noise ratio.

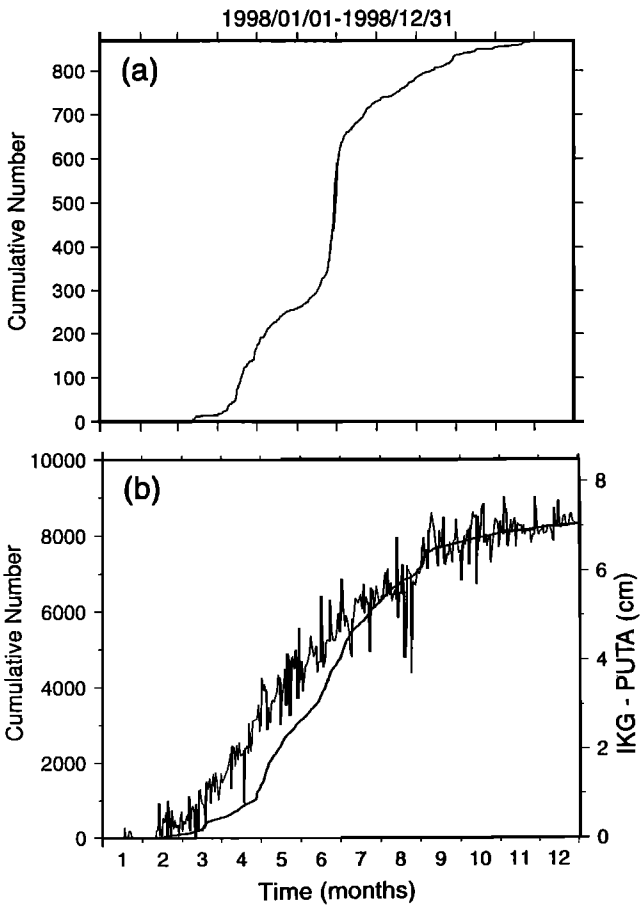

Figure 3. (a) Cumulative number of the VLP events observed at GNB in 1998. (b) Cumulative number of volcanic earthquakes around Iwate Volcano (thick curve) and temporal variations of horizontal distance (perturbed thin curve) between PUTA and IKG (see Figure 1) detected by the GPS measurement (data are from Tohoku University, [1999]).

Figure 6 shows the borehole strain and tilt records at GNB associated with the VLP. The volumetric strain records also show a dominant period of 10 s and duration of 30-60 s, which is quite similar in waveform to the displacement seismogram of VLP. This suggests that the long-period waves mainly consist of the compressional elastic waves. We also find that some of the VLPs accompany a gradual DC change of volumetric strain simultaneous with the occurrence of VLP. For example, events in Figures 6a and 6b brought about DC offset of roughly -10^{-10} and 10^{-10}, respectively, as shown by arrows. However, many VLP do not show any significant level changes of strain as shown in event in Figure 6c. The tilt records also indicate 10 s oscillations associated with the VLP, but no significant level changes of tilt are observed. These results suggest that there are no simple systematic static changes in the strain and tilt. However, it is noteworthy to mention that some of the VLPs (July 7, June 28 1830 LT, and August 19; the latter two are not shown in Figure 6) accompany significant DC change of $\sim 10^{-10}$ for strain and $< 1.5 \times 10^{-9}$ radian for tilt at GNB station.

Figure 7 shows particle orbits of VLP recorded at GNB station. All of the orbits show elliptical shapes, and their major axes are directed to the north-northwest with a dip of 30°-40°. We do not see any significant temporal changes of the particle orbits for the events observed from April to August 1998. This suggests that a common process causing the VLP continued beneath the volcano for almost a half year at the same location. In Figure 8 we display particle orbits at all stations, where the orbits are projected on the horizontal plane. The orbits at all of the five stations indicate elliptical shapes, and their major axes, which are shown by broken lines, are directed to the south of peaks 4 and 5 of the volcano. On the basis of this observation, together with the *P* wave nature of VLP, we infer that the hatched region, where the dashed lines intersect, is the source region of VLP. The source depth of VLP is estimated to be a few kilometers from the dip angle of the major axis of GNB orbits and the distance from the station to the intersection area. The estimated source location can well explain the particle orbits observed at the MTI station, which is located just above the source region.

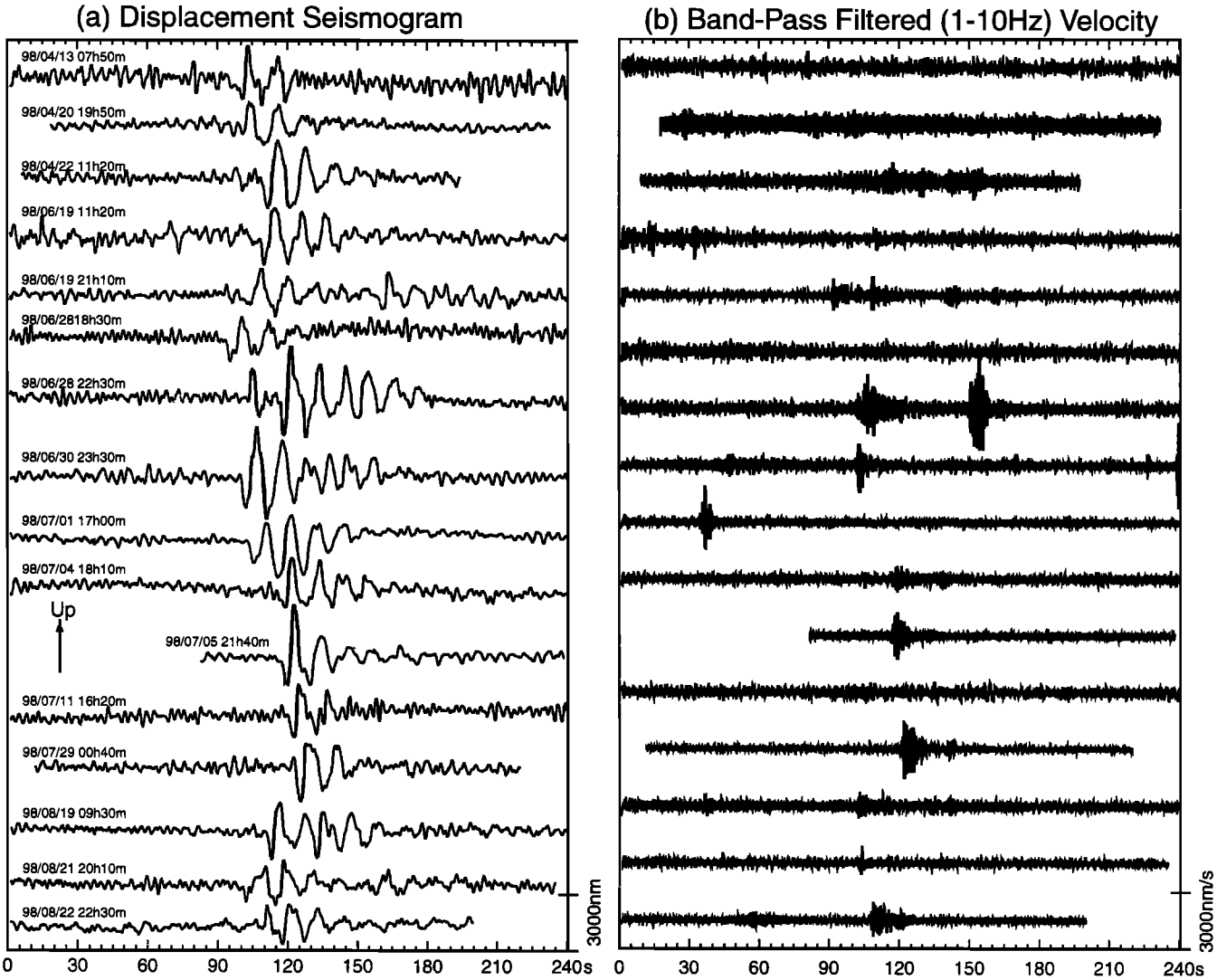

Figure 4. (a) Examples of displacement seismograms of the VLP observed for the period from April to August 1998. (b) Short-period seismograms that are obtained by filtering the broadband signals from 1 to 10 Hz.

4. Semblance Analysis

The source region estimated from an analysis of particle orbits in section 3 is considered to represent a centroid of the source because the major axes of the particle orbits are controlled by phases having large amplitudes. In this section, to clarify further the detailed structure of the source region of each VLP, we apply the semblance analysis similar to procedures used in previous studies [e.g., *Furumoto et al.*, 1992; *Ohminato et al.*, 1998].

We first postulate that a VLP isotropically radiates spherical waves from a point source and that the waves propagate in a semi-infinite uniform structure with a velocity of V. Then, we calculate semblance coefficients C for an assumed point source located at (x_0, y_0, z_0):

$$C(x_0,y_0,z_0)=\frac{\sum_{j}^{M}\{\sum_{i}^{N}u_i[t_j+\Delta t_i(x_0,y_0,z_0)]\}^2}{\sum_{j}^{M}\sum_{i}^{N}u_i^2[t_j+\Delta t_i(x_0,y_0,z_0)]}, \quad (1)$$

where N represents the number of station, u_i is the velocity amplitude of the vertical component for the ith station, Δt_i (x_0, y_0, z_0) is the travel time from the assumed source to the ith station, t_j is the discretized time, and M is the number of the data for each station. We set point sources with an interval of 1 km for vertical, east-west, and north-south directions and calculate semblance coefficients for each point source. Then, we take the point source having the maximum semblance coefficient as the hypocenter of VLP.

To examine whether the hypocenter of each VLP migrates or not during its oscillation, we shift time windows with a width of 20 s by every 10 s from the beginning to the end of the events and calculate the semblance coefficients for each time window (Figure 9). We use vertical components of the velocity seismograms at the six stations that are band-pass filtered for a period from 8 to 12 s. The wave velocity V is assumed to be 2.5 km/s in which the maximum semblance coefficient is obtained.

In Figure 10 we show contour maps of the semblance coefficient at a depth of 0 km for each time window. We could

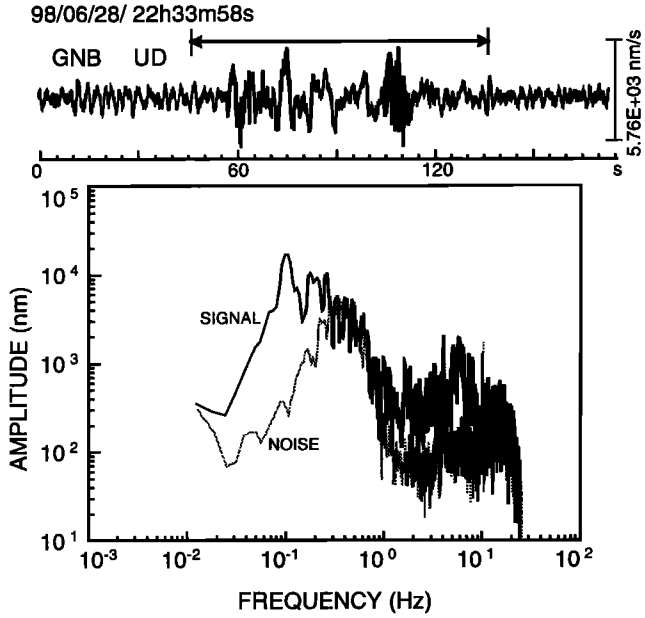

Figure 5. Velocity spectra of the VLP (solid line) and ground noise (dashed line) for the event on June 28, 1998. Time window for the noise spectrum is set at the waveform before the signal.

not resolve well the depth of the hypocenter probably because of the limited numbers of seismic stations and poor knowledge of seismic velocity structures. However, the results obtained for 0-4 km show similar characteristics, so that horizontal location of the source is reliable. It is found that the hypocenter for the first time window (0-20 s) is located at the south flank of peak 3, and that the hypocenter migrates westward to the south of peak 4 by the end of the event. The westward migration of the source is supported by the directivity effect that is seen in the observed waveform as shown in Figure 9. That is, the first trough of the waves observed at MTI arrives 1 s later than that of MTK and GNB stations (see first dashed line) while the second peaks of MTI arrives 1 s earlier than the others (as denoted by the second dashed line). Since MTI is located at the west of the source region, the observed differences of the arrival time are explained by the westward migration of the source. We analyze other VLP events by applying the same semblance analysis and find that the source of VLP is distributed at a shallow depth beneath southern flank of peaks 3-5.

The westward migration of the source, however, might be an artifact caused by our simple assumptions that each VLP has a point source isotropically radiating seismic waves and that there are no plural sources at the same time. Hence, in the following section, we investigate the moment tensor of VLP to examine whether the apparent westward migration is real, as well to clarify the source mechanism of VLP.

5. Moment Tensor Inversion

Moment tensor inversion analyses are often done by assuming a source time function expressed as a simple mathematical function, e.g., a ramp function. However, VLP events observed at Iwate Volcano seem to have complicated source time functions. In such a case, it is better to determine both the moment tensor and the time functions simultaneously. In this study, we use an inversion method similar to that of the previous studies by *Ide et al.* [1996] and *Ohminato et al.* [1998] because their methods are very useful for the case when the source time function cannot be assumed beforehand.

Since the VLP source region migrates westward beneath the south flank of peaks 3-5, we approximate the VLP source as a superposition of plural point sources set at these regions. The candidates of source location are put at grid points of gray lines in Figure 1. We represent the position of each grid point by a Cartesian coordinate system with the origin at the summit of Iwate Volcano (Yakushi-dake; 39.504°N, 140.005°E), where north, east, and downward vertical are positive. For example, the position of (-3, -5, 3) corresponds to a grid located at 3 km south, 5 km west of the summit, and 3 km deep from the sea level. We determine six moment tensors (M_{xx}, M_{yy}, M_{zz}, M_{xy}, M_{yz}, and M_{xz}) for each grid point, where subscripts x, y, and z represent the direction of north, east and depth, respectively. We denote the observed displacement as $O_{ij}(t)$ and the Green's function of each component as $C^{r}_{ij,pq}(t)$, where i represents the station, j is the component, p and q are the components of six moment tensors,

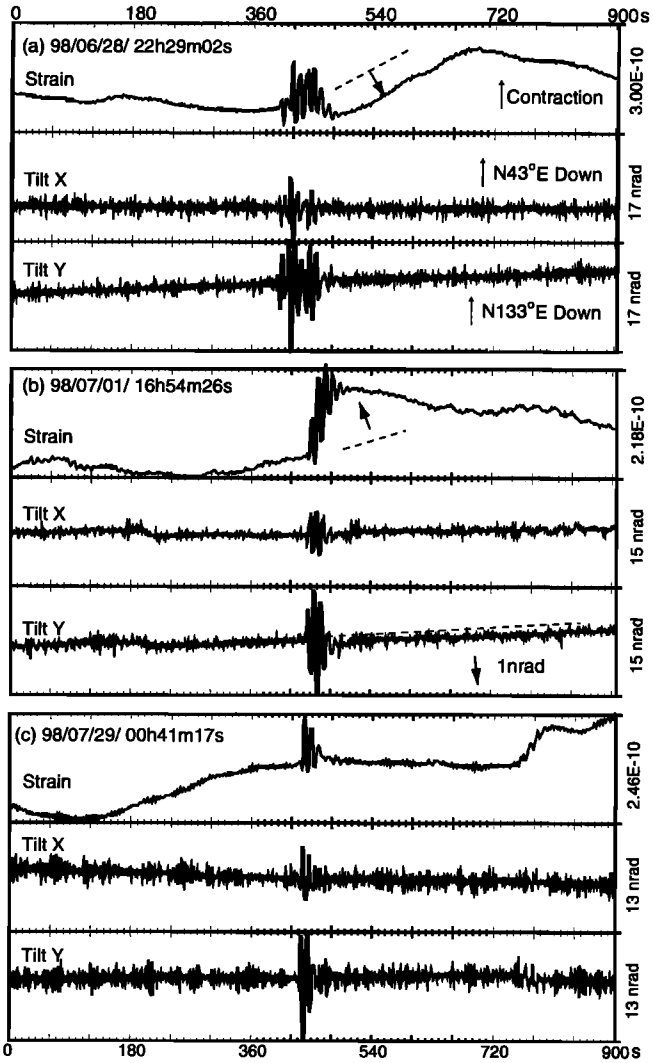

Figure 6. Examples of strain and tilt records associated with very long period seismic events. Full-scale values of tilt and strain are shown at the right side of each trace.

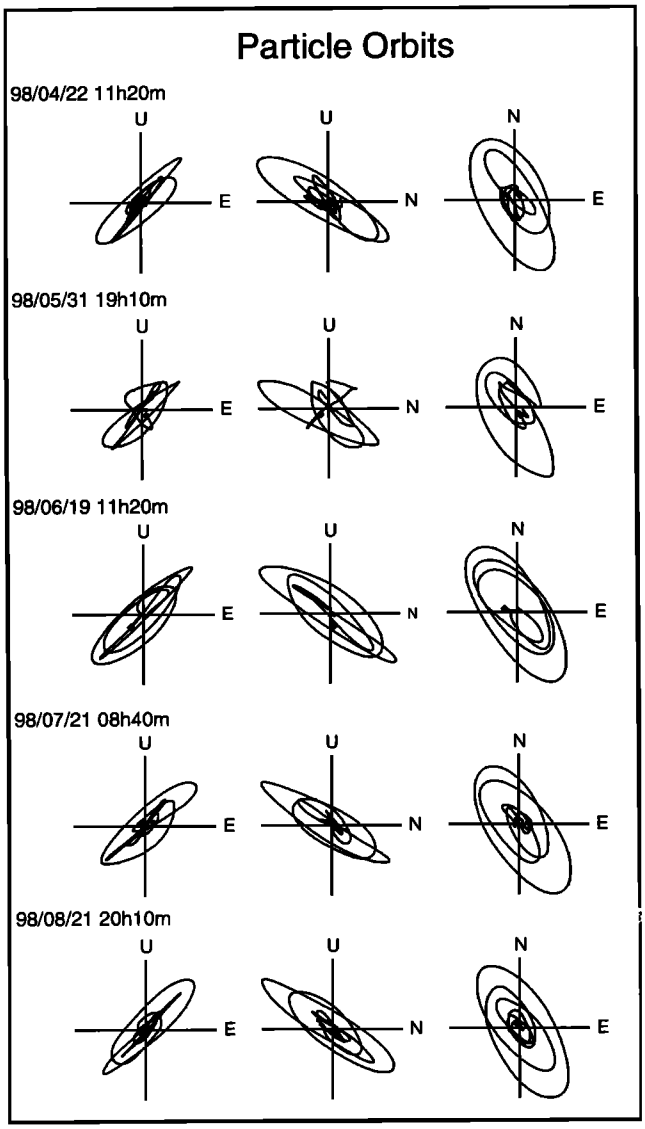

Figure 7. Particle orbits of VLP waveforms recorded at GNB station for the period from April to August 1998. All of the particle orbits have elliptical shapes, and no significant temporal changes are observed.

and r is the point source number. We determine the bestfit solutions of moment tensors by minimizing the residual:

$$S=\sum_{k}^{K}\sum_{i}^{N}\sum_{j}^{3}[O_{ij}(k\delta t)-\sum_{r=1}^{R}\sum_{p=1}^{3}\sum_{q=1}^{3}\sum_{l=0}^{L}C^{r}_{ij,pq}(k\delta t-l\delta t)M^{r}_{pq}(l\delta t)]^2, \quad (2)$$

where δt is the sampling interval, N is the number of stations, K is the number of data for each component of the station, L is the number of time points to determine the moment tensors, R is the number of point sources, and M^{r}_{pq} is the moment of pq component for rth point source. We obtain the best solutions of moment tensor time functions that minimize the residual by using the least squares method.

We apply the moment tensor inversion to a VLP that occurred at 0047 LT on July 29, 1998, because of good signal to noise ratio in the three components at all six stations. Owing to the limited number of available stations we approximate the seismic source of the VLP by two point sources. We assume, for simplicity, that the two point sources are located at grid points in Figure 1 (the grid points are also distributed vertically every 1 km) and that they are separated only in the east-west direction (x and z coordinates are the same). Thus we use 18 components of the observed seismograms to determine the temporal variations of the six moment tensors ($M_{xx}(t)$, $M_{yy}(t)$, $M_{zz}(t)$, $M_{xy}(t)$, $M_{yz}(t)$, and $M_{xz}(t)$) for each of the two point sources. Green's functions of the six components of moment tensor for each set of the sources and stations are calculated by using the discrete wavenumber method [*Bouchon*, 1981] with a reflection and refraction coefficient matrix [*Kennet and Kerry*, 1979] and then are convolved with the response function of the STS-2 seismometer. We assume a horizontally layered structure shown in Table 1, following the velocity structure around Iwate Volcano used for the hypocenter determination by *Tanaka et al.* [1999a]. We bandpass filter the observed velocity seismograms for 8-12 s, integrate them to obtain displacements, and then resample them every 1 s. Fitting the synthetics with the observed displacements for duration of 80 s (i.e., K =80), we obtain the bestfit solutions of the moment tensors for 70 s (L=70). Then, we calculate the residuals S for each pair and obtain the pair having the minimum residual S as the best point sources.

An example of the residual for source pairs is shown in Table 2. The best dual sources are obtained at locations of (-2, -10, 2) and (-2, -6, 2), which are consistent with the hypocenter regions determined from the orbit analysis. Figure 11 shows temporal variation of the moment tensors for the best two sources. It is found that the diagonal components (M_{xx} and M_{yy}) of moment tensors are dominant for both of the two point sources, although small amplitude of M_{yz} is also recognized for the source at (-2, -10, 2). The moments oscillate for 30 s with a period of ~10 s. Time functions of

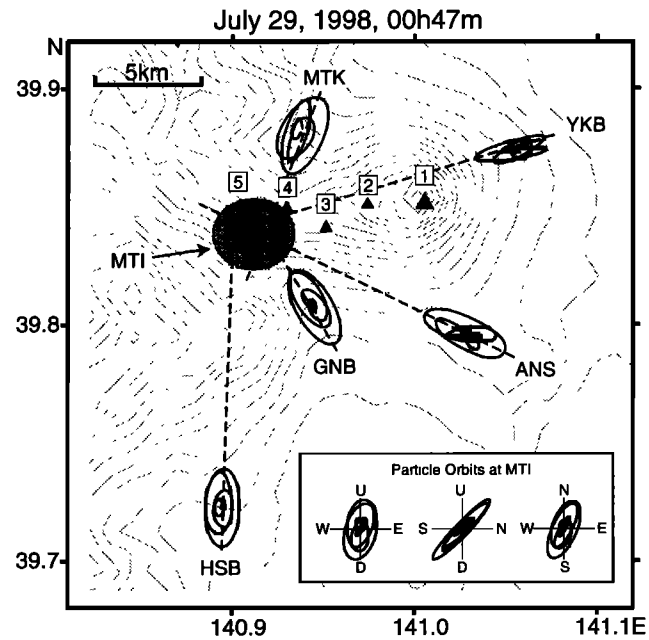

Figure 8. Particle orbits of VLP at the five stations (projected on the horizontal plane). The hatched ellipse is the VLP source area inferred from the intersections of major axes of the particle orbits. Since MTI (plus) is located in the hatched area, the orbit is plotted at the bottom of Figure 8.

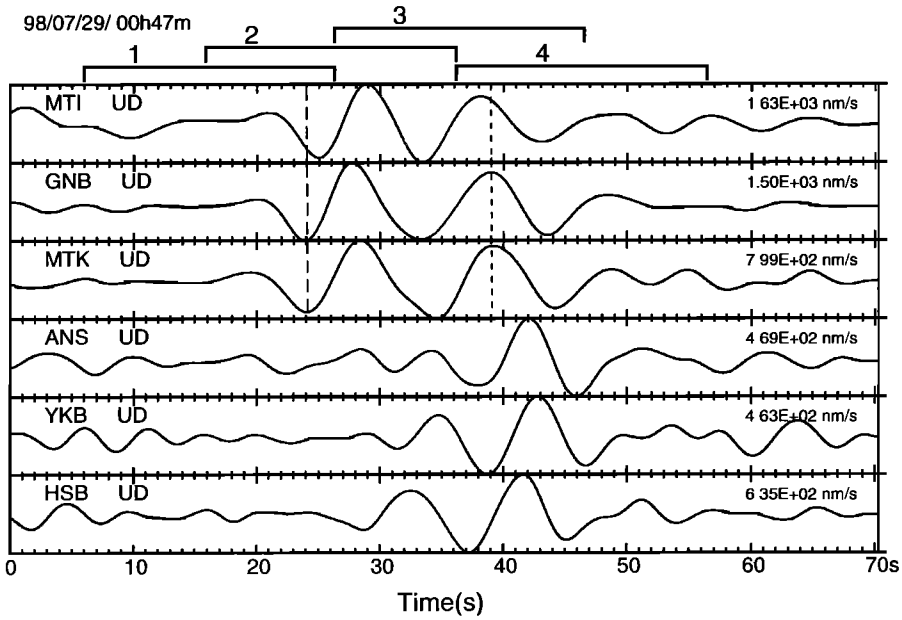

Figure 9. Band-pass filtered (8-12 s) velocity seismograms of the vertical component at the six stations for the event on July 29, 1998. Note that the first trough of the waveforms for MTI arrives ~1 s later than those for GNB and MTK while the second peak for MTI is observed 1 s earlier than the others. Time windows set for the semblance analysis of MTI seismogram are shown at the top: 1, 2, 3, and 4 correspond to the time windows of 0-20, 10-30, 20-40, and 30-50 s, respectively, in Figure 10.

M_{xx} and M_{yy} for each point source are almost in phase. This means that significant volume changes (i.e., deflation and inflation) occur a few times in ~30 s at the source regions. Comparing the moment tensor functions for each point source, we further find that phases of the source (-2, -6, 2) are out of phase of (-2, -10, 2). That is, the deflation and inflation mutually occur at the two point sources that are 4 km apart from each other.

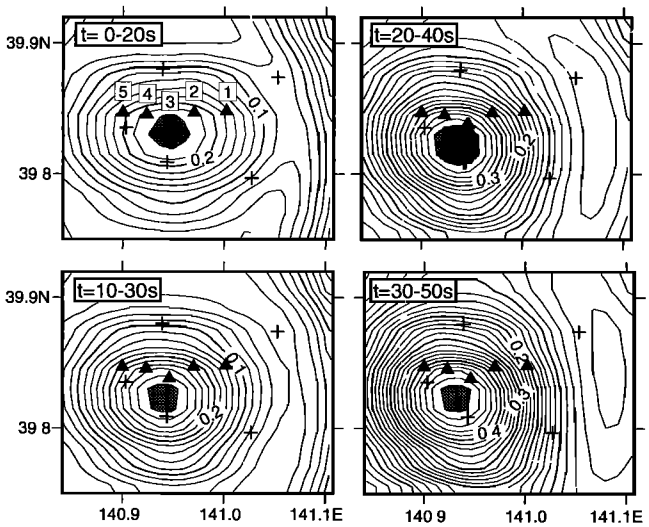

Figure 10. Contour maps of the semblance coefficients for the event on July 29, 1998. Contour maps for 0-20 s, 10-30 s, 20-40 s, and 30-50 s correspond to the time windows of 1-4 in Figure 9, respectively. The hatched area is the region having the maximum semblance coefficient (i.e., source position) for each time window. All of the contour maps are the results for a depth of 0 km.

Maximum amplitude of M_{xx} is a little larger than the other two diagonal components (M_{yy} and M_{zz}) for the best pair. This may represent a source of opening and closing of a dike elongating to the east-west direction with a dip of 90°. The strike of dike is consistent with the other observation. For example, peaks of Nishi-Iwate align in the east-west direction, and most of volcanotectonic earthquakes observed at Nishi-Iwate show a strike-slip mechanism in which one of the nodal planes strikes east-west [*Tanaka et al.*, 1999a). The maximum moment is estimated to be 2 x 10^{13} Nm in M_{xx} component.

In Figure 12 the synthetic seismograms predicted from the best moment solutions are compared to the observed displacements. The synthetics well explain both amplitudes and phases of the observed displacements from the beginning to the end of event at the all stations. Variance reduction of the solution reaches > 95%, which indicates a very good fit of the synthetics to the observed seismograms. Although we do not analyze other VLP events owing to lower signal to noise ratio, the same source mechanism should apply since all the VLPs have similar waveforms.

6. Discussion

6.1. Stability of the Moment Tensor Solution

We have taken two point sources to represent the VLPs since results of the semblance analysis show an extent of the source region in the east-west direction. However, one point source might be sufficient to model the VLP source. Hence we conduct a moment tensor inversion assuming only one point source to compare the result with the solution of the two point sources (two-point source model). Applying the same inversion algorithm used for the two point sources, we obtain the best location of the one point source to be at (-3, -8, 3). This is located nearly at the middle of the best pair for the two

Table 1. Horizontal Layered Structure Used for Calculating Green's Functions

Layer	Density, g/cm^3	*P* wave velocity, km/s	*S* wave velocity, km/s	Thickness, km
1	2.0	2.50	1.40	0.1
2	2.0	3.17	1.79	0.9
3	2.2	4.52	2.60	1.0
4	2.4	5.60	3.26	4.0
5	2.5	5.92	3.45	8.0
6	2.6	6.65	3.87	17.0
7	3.2	7.20	4.19	infinite

point sources. The moment tensor functions are shown in Figure 13. Similar to the two-point source model, deflation and inflation dominate for 30 s. M_{yz} component is also observed. Figure 14 compares the observed displacements with the bestfit synthetics. The synthetics explain fairly well the observed seismograms. However, the phases and amplitudes are inconsistent for several components, such as NS component of GNB and EW component of MTK, YKB, and HSB. Variance reduction is 75%. Since the numbers of the model parameters are different, we use the Akaike Information Criterion (AIC) [*Akaike*, 1973] to examine which model is appropriate for the VLP source mechanism. The AIC value for the two-point source model is estimated to be 17,671 while the AIC for the one-point source model is 19,605. Since the model having the smaller AIC value is statistically better, we conclude that the two-point source model is more plausible for representing the VLP source. Observed westward migration of a point source in section 5 (semblance analyses) is also considered to be an artifact due to our single point source approximation.

We have shown that the two-point source model is better than one-point source model, but there may be a trade-off in the moment solutions between the two sources. If so, mutual deflation and inflation may be artificial due to our approximation of the source. Hence we check the resolution of our solution by following simulation analysis. First, we synthesize displacement waveform for a single source located at (-3, -8, 3) that has a triangular source time functions with a width of 10 s and peak amplitude of 1 N m only for the diagonal components (i.e., M_{xx}=M_{yy}=M_{zz}= 1 N m, M_{xy}=M_{yz}= M_{xz}= 0 N m). Then, we estimate the moment tensor solutions

Table 2. Residuals for Pairs of the Two Point Sources

Location of Source 1	Location of Source 2						
	5	6	7	8	9	10	11
4	3.04	2.66	2.58	2.45	2.06	1.74	2.21
5	-	2.45	2.47	2.22	1.73	1.33	1.65
6	-	-	2.28	1.70	1.37	1.00	1.20
7	-	-	-	1.46	1.35	1.03	1.21
8	-	-	-	-	2.02	1.32	1.50
9	-	-	-	-	-	1.74	1.77
10	-	-	-	-	-	-	2.04

Numbers in locations of source 1 (4-10) and source 2 (5-11) represent the distances in the east-west direction from the origin in kilometers. The residuals for each pair are normalized by the minimum value obtained for the pair at (-2, -6, 2) and (-2, -10, 2). All of the sources shown are set at 2 km south of the origin and at a depth of 2 km.

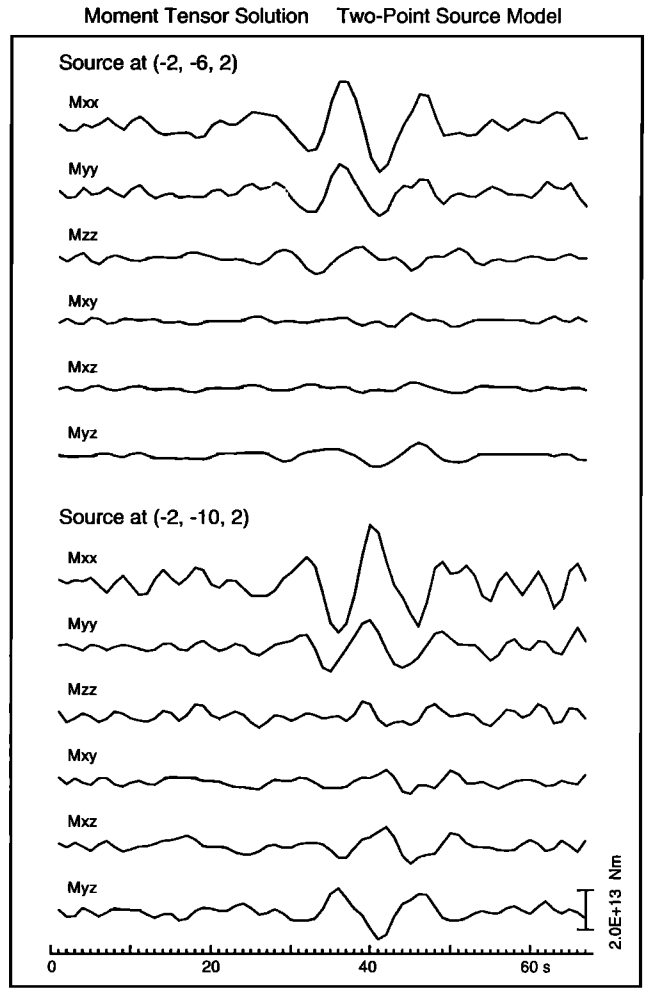

Figure 11. The best solution of moment tensor time function for the two point source. The sources are located at (-2, -6, 2) and (-2, -10, 2).

assuming two sources at (-2, -6, 2) and (-2, -10, 2), which are the locations of the best solution. The solutions obtained for the two point sources are shown in Figure 15. We find that M_{xx} and M_{yy} at (-2, -6, 2) show a triangular function similar to the assumed source. However, their peak amplitude (~0.5) is much smaller than the assumed one, and M_{zz} is hardly observed. The solutions at (-2, -10, 2) show smaller amplitude for all of the components. This simulation result indicates that there is no significant trade-off between the two sources of the two-point source model. Therefore, we conclude that the mutual deflation and inflation motion is not an artifact of our approximation of the source.

We have so far examined the time functions of six moment tensors, but single forces may be candidates for representing the source mechanism of VLP. We therefore carry out the waveform inversion in which time functions of the six moment tensors and three single forces (F_x, F_y, and F_z) are simultaneously determined. Assuming one-point source at (-3, 8, 3), we obtain the solutions. The result shows a variance reduction of 86%, and the AIC is estimated to be 19,184. Therefore single-force sources are not significant in the source mechanism of VLP.

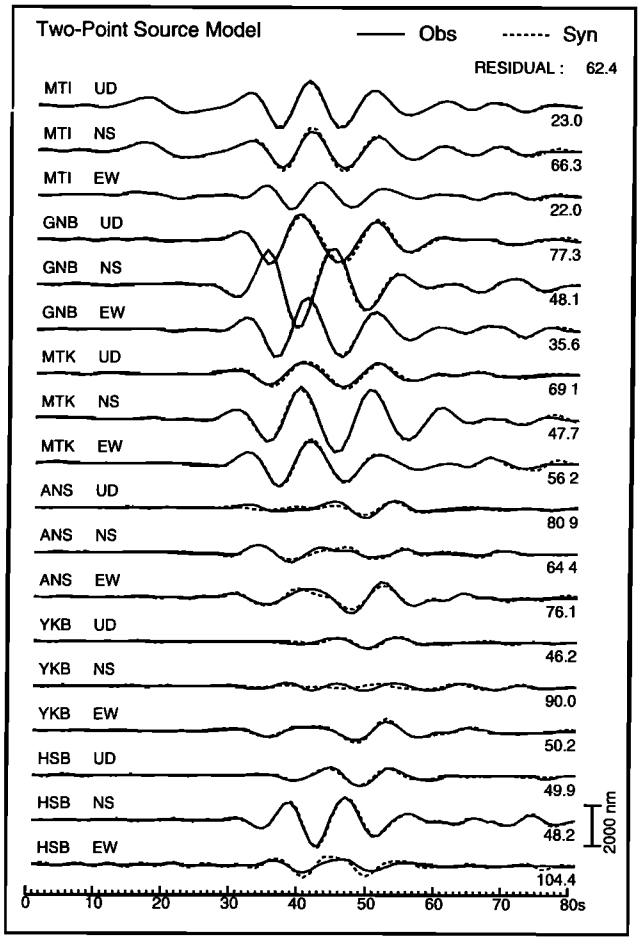

Figure 12. Comparison of the synthetic seismograms (dashed lines) with the observed displacement (solid lines) for the best two point sources. The values shown on the right of each trace show residuals (unit is nanometers) between the synthetics and the observed seismograms. Variance reduction is estimated to be > 95%.

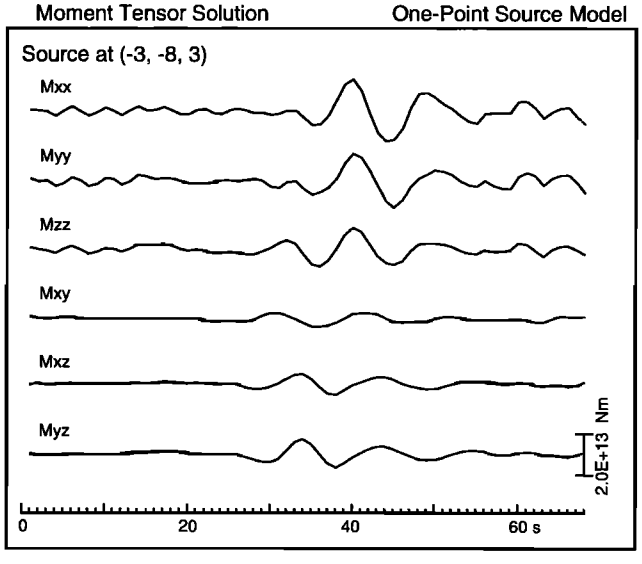

Figure 13. The best solution of moment tensor time function for the single-point source. The source is located at (-3, -8, 3).

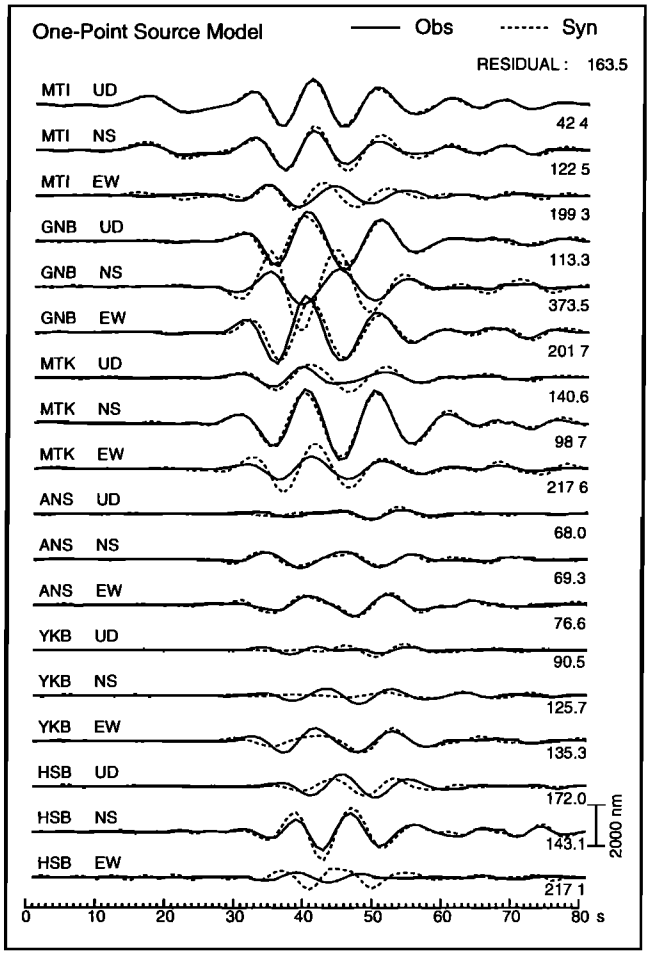

Figure 14. Comparison of the synthetic seismograms (dashed lines) with the observed displacement (solid lines) for the single-point source. Variance reduction is 75%.

6.2. Comparison With Results of Other Geophysical Studies

We have so far examined activities and source characteristics of VLP. They are summarized as follows: (1) VLP activity is intense from April to August 1998. (2) The source region is 2 km deep and 2 km south of peaks 3-5 (Inukura-yama, Ohmatsukura-yama, and Mitsuishi-yama). (3) There are no significant changes of the location for the period from April to August 1998. (4) VLPs are excited by mutual deflation-inflation motion. (5) VLPs accompany short-period seismic signals at the beginning and at the end of event. To clarify the source process of VLP, we first compare these results with other geophysical and geological studies on Iwate Volcano, such as activity of volcanotectonic earthquakes, crustal deformations, velocity structure, and so on.

For the period from April to August 1998, when VLP activity was most intense, the seismic activity at the shallow part of the volcano was quite high, and rapid crustal deformations were also observed (Figure 3). *Tanaka et al.* [1999a] reported an extenstion of the hypocenters of volcanotectonic earthquakes from the west of Higashi-Iwate to Mitsuishi-yama. *Ueki et al.* [1999] applied the Mogi model to the crustal deformation data obtained by GPS and indicated that the center of spherical pressure sources migrated from a depth of 5 km beneath the west of Higashi-Iwate to a depth of

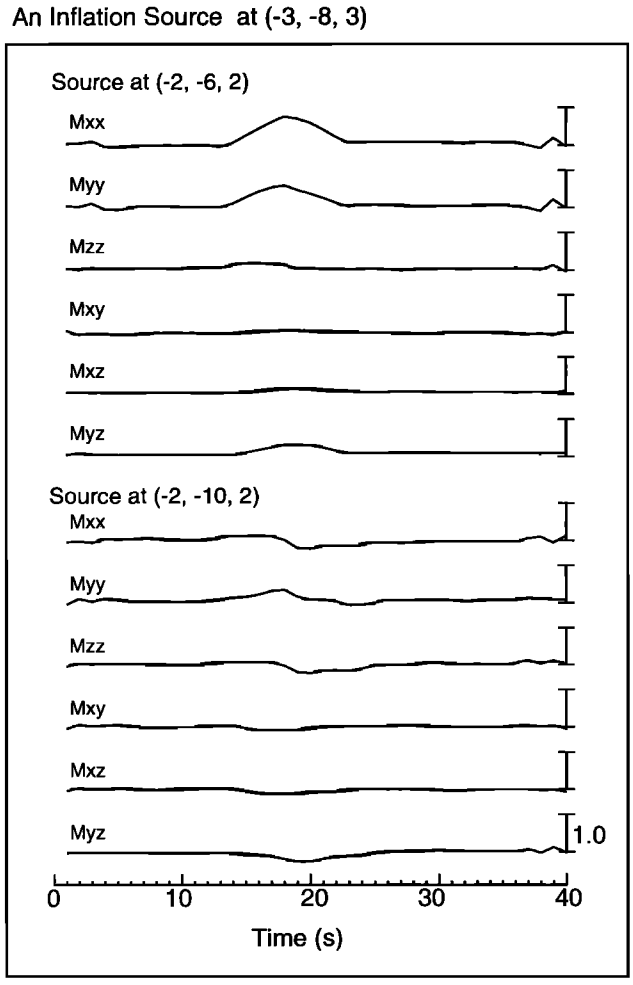

Figure 15. Moment tensor time functions obtained from the inversion of simulation data (see text for details).

2.5 km beneath the west of Nishi-Iwate for the same period. Their results suggest that magmatic fluid ascended from a deep part of the volcano and migrated westward when VLP was most active. *Sato and Hamaguchi* [1999] also analyzed borehole tilt and strain data recorded at GNB, ANS, and YKB together with GPS data. Fitting theoretical deformation fields to the observed ones, they postulated two pressure sources: one is a dike elongating in the east-west direction from peaks 1 to 3, and the other is a spherical pressure source that persisted at 4 km depth beneath the southern flank of peak 5 (Figure 16). The western edge of the dike is located at the eastern region of the VLP source. The spherical pressure source is situated at a depth of 4 km, adjoining the VLP source region. However, the depth accuracy is not very high since they did not use the data from close to the source region [M. Sato, personal communication, 1999]. Allowing for estimated errors, the spherical pressure source may coincide with the western edge of our VLP source. These results suggest that VLP is closely related to the activity of pressure sources beneath the volcano.

Recently, *Tanaka et al.* [1999b] obtained a three-dimensional velocity structure at shallow parts of Iwate Volcano by using first P and S wave arrival times of natural earthquakes. Their result shows that a low-velocity region of P and S waves coincides with the location of the VLP source and that the region shows a higher V_P / V_S ratio (2.0). This result strongly suggests the existence of magmatic fluid such as hot water and/or magma at the VLP source region. Several other studies of structure of Nishi-Iwate also suggest the existence of fluid in the same area. Regions having low electric resistance are detected at shallow depths of the south of peaks 1-3 and borehole log data indicate an existence of hot water zones at a depth of 400 m south of peak 4 [e.g., *Doi*, 1999]. Therefore we infer that the magmatic fluid plays a very important role in the excitation of VLP.

6.3. Source Process of the Very Long Period Seismic Events

Considering the source mechanisms obtained from our inversion and the results of other geophysical studies, we propose a source model of VLP as illustrated in Figure 17. There are two chambers of magmatic fluid at a shallow region around peak 4, which are connected to each other by a narrow channel. One of the chambers (probably the eastern one) is gradually pressurized by an upward migration of magmatic fluid from a deeper part. When the pressure reaches a critical level, the narrow channel opens and excites high-frequency seismic waves. As a result, pressure waves and/or masses of the fluid horizontally migrate to the other chamber. Owing to the resonance of the chambers and conduit [e.g., *Chouet*, 1988] and/or the characteristics of the nonlinear flow [*Julian*, 1994] the fluid oscillates with a period of ~10 s. This long-period oscillation of fluid in the chambers and conduit are detected as a VLP. When the pressure and/or mass balance reaches equilibrium, the channel closes and again excites high-frequency waves. The high-frequency signals observed at the beginning and the end of VLP are interpreted to be generated by opening and closing of the valve. This process repeatedly occurs so that magmatic fluid is transferred from the east to the west, as was detected by geodetic measurements [*Ueki et al.*, 1999].

In the following, we formulate the model of Figure 17 to explain quantitatively the nature of VLP by periodic mass transformation of magmatic fluid. We assume that two pressure chambers, which have volumes of V_1 and V_2, respectively, are filled with a fluid having bulk modulus of K. Pressures of the two chambers are expressed by P_1 and P_2, respectively. The chambers are connected to each other by a narrow channel with a length of L and a cross-sectional area of A. The volume of chambers is so large that flow velocities in the chambers are negligible compared with that in the conduit and that deformations of the conduit and chambers are too small to affect the flow motions in the reservoir system. Then, from the equation of the momentum conservation, the flow velocity v in the conduit is expressed as

$$\frac{\partial v}{\partial t} + v\frac{\partial v}{\partial s} = -\frac{1}{\rho_f}\frac{\partial P}{\partial s} - 2\alpha v, \qquad (3)$$

where s represents the direction of flow, ρ_f is the density of fluid, and P is the pressure in the conduit. Parameter α represents the attenuation factor due to the viscosity of fluid, and $\alpha = 4\pi\mu/\rho_f A$ for a cylindrical pipe and $\alpha = 6\mu/\rho_f d^2$ for dike, where μ is the viscosity of fluid and d is the thickness of the dike. The temporal variation of pressure in the chambers is related to the flow as

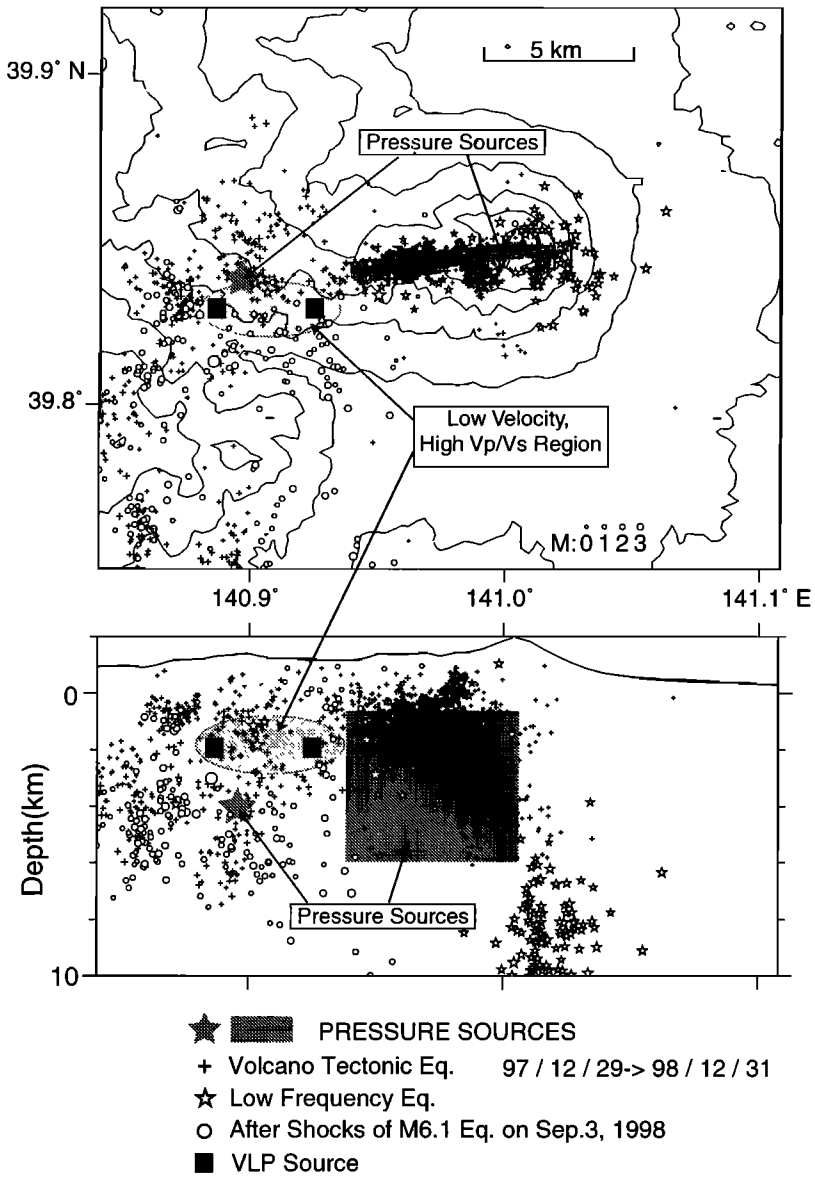

Figure 16. Comparison of locations of the very long period events with those of a spherical and a dike-shaped pressure sources [*Sato and Hamaguchi*, 1999], hypocenters of volcanotectonic events and low-frequency events, and low-velocity zone [*Tanaka et al.*, 1999b].

$$\frac{\partial P_1}{\partial t} = K\frac{Av}{V_1}, \qquad \frac{\partial P_2}{\partial t} = -K\frac{Av}{V_2}. \tag{4}$$

We focus on the macroscopic fluid motions between the two chambers and neglect small fluctuations of the flow in the conduit. Substituting $\partial v/\partial s=0$ and $\partial P/\partial s = (P_1-P_2)/L$ in (3) and (4), we obtain the damped oscillation of the flow as follows:

$$v = v_0 \exp(-\alpha t)\sin(\sqrt{1-(\alpha/\omega_0)^2}\,\omega_0 t + \theta'), \tag{5}$$

$$\omega_0 = \sqrt{\frac{KA}{\rho_f L}\left(\frac{V_1+V_2}{V_1V_2}\right)}, \tag{6}$$

and v_0 and θ' are parameters determined from an initial condition. Since the flow velocity in the conduit oscillates periodically, the two chambers mutually inflate and deflate to excite long-period waves. Dominant period of the oscillation ($T_0=2\pi/\omega_0$) is controlled mainly by the configuration of conduit, the volume of chambers, and magma properties, when $\alpha << \omega_0$. For example, large volume of a chamber with a narrow channel excites a longer-period wave, and fluid having large bulk modulus (i.e., low compressibility) excites a shorter-period wave. For the VLPs at Mount Iwate the observed dominant period, T_0=10 s, can be explained by substituting in (6) appropriate values, for example, $V_1 = V_2 = 10^5$ m^3, L=4000 m, and $(K/\rho_f)^{1/2}$ = 900 - 2800 m/s for A = 10-100 m^2. The attenuation factor α is estimated to be ~0.05/s because the periodic oscillation lasts for a few cycles. Hence we obtain the kinematic viscosity (μ/ρ_f) of 0.04-0.4 m^2/s for a cylindrical channel with A = 10-100 m^2 and 10^{-6}-10^{-2} m^2/s for a dike with d = 0.01-1 m. The observed kinematic viscosity may be explained by magma with $\mu=10^2$-10^3 Pa s and ρ_f=2500 kg/m^3 and/or water (~10^{-6} m^2/s).

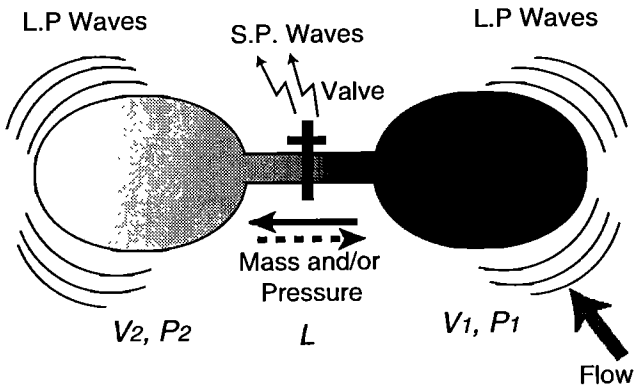

Figure 17. A schematic illustration of source process of the very long period seismic event.

We can also relate the seismic moment M_0 to this model. The seismic moment for each chamber can be expressed as $2K\delta V$ for the case of a spherical chamber [e.g., *Nishimura*, 1998], where δV is the volume of fluid poured into a chamber from another one for a half cycle of the oscillation. Hence we obtain

$$M_0 = \int_0^{\pi/\omega} 2KAv\,dt = \int_0^{\pi/\omega} 2KAv_0 e^{-\alpha t}\sin\omega t\,dt$$
$$= 2KAv_0\frac{\omega(1+e^{-\pi\alpha/\omega})}{\alpha^2+\omega^2}, \quad (7)$$

where v_0 is the maximum velocity of the flow. Since M_0 and ω are observable parameters, we can estimate the energy flow rate Kav_0 which indicates the power of the magmatic fluid flow that excites a VLP. For the VLP observed on July 29, 1998, M_0 =2 x 10^{13} N m, ω=2π/10 /s, and α=0.05/s so that KAv_0 is estimated to be 3.6 x 10^{12} J/s. If K is 10^{10} Pa and v_0= 36 m/s, A is estimated to be 100 m^2. The energy flow rate of the VLP is one third of that for an explosion earthquake (9 x 10^{12} J/s) observed at Sakura-jima Volcano [*Nishimura*, 1998]

In this model, we have assumed no convection and no spational variation of fluid velocity in the conduit. This implies that density of fluid is constant in the conduit and no acoustic waves propagate between the chambers. Thus our model is in a marked contrast to resonance models in which acoustic wave propagation is mainly considered [e.g., *Crosson and Bame*, 1985; *Fujita et al.*, 1995]. Since our inversion results do not show significant single forces for the VLPs, we did not consider the excitation of single forces from the channel, as proposed by *Ukawa and Ohtake* [1987], in which a low-frequency event observed at Izu-Ooshima is modeled by periodic oscillations of magma flow in the channel. To evaluate the effect of convection in the channel and chambers and to examine which force systems are dominant for seismic wave excitation, numerical simulations including couplings of the fluid and elastics would be necessary. However, our model succeeds in physically accounting for the most important natures of VLP. The energy flow rate derived from the model provides a basic parameter for expressing the magnitude of VLP in terms of flow dynamics of magmatic fluid beneath volcanoes.

Finally, we compare the observed static deformation field with the theoretical ones predicted from the present source model. After the periodic oscillation of the fluid, the eastern chamber deflates and the western inflates. Since station GNB is located close to the eastern chamber, the strain and tilt are mainly affected by the dilatation of the eastern chamber, which has a moment of $-M_0/2$ (when $\alpha \ll \omega_0$). Then, we can roughly estimate the theoretical deformation field from the observed seismic moment (10^{13} N m) by approximating the source as an isotropic deflation. For the events of July 7, June 28 (1830 LT), and August 1? (the latter two are not shown in Figure 6) the observed static contraction in the strainmeter shows almost a half of the maximum amplitude of the periodic oscillations. The observed tilt indicates a summit deflation with a magnitude of ~1 nrad (see y direction in Figure 6b). These observations are well consistent with the static deformation predicted from the isotropic dilatation. The observed amplitude of periodic oscillations in the tilt is, however, 1 order larger than the prediction, which may be due to a site effect, an effect of topography, and unknown magmatic process.

Although the three VLPs can be explained by the present source model, other VLPs do not accompany significant static changes in the strain and tilt, and the event of June 28 in Figure 6a seems to indicate static dilatation after the event. These observations imply that the VLPs do not accompany a simple systematic change of the static deformation field. The reasons why such variety of the static deformation is observed are not clear because of the limited number of available data. However, the reasons could be related to (1) a complexity of spatial distribution of strain fields, (2) an existence of other small chambers that are not detected by seismic analyses, and (3) unknown additional magmatic fluid migrations. For example, even in a simple case of an isotropic pressure source, polarity of the volumetric strain changes from dilatation to contraction at the locations (nodes) whose horizontal distance from the source is ~1.5 times of the source depth. Actually, station GNB is located very close to such a node (the horizontal distance from the eastern source is 2.6 km and the source depth is 2 km). The reservoir system seems to temporally change the configuration since the observed seismic waveforms of the VLPs are a little different from each other (see Figure 4). Such complexity of the reservoir system and the deformation field may cause nonsystematic changes of the static deformation field associated with the VLP event. However, to discuss the origins in more detail, we need to analyze a dense network data of strain and tilt meters around the source region.

7. Conclusion

We observed very long period seismic events of 10 s period associated with the 1998 activity of Iwate Volcano, although there were no significant surface phenomena, such as steam explosion, ash effusion, and so on. We have examined the waveform characteristics and source process of the events from broadband seismograms at six seismic stations located around the volcano by using a semblance analysis and moment tensor inversion. The main results are summarized as follows; (1) The activity of VLP was most intense for the period from April to August 1998, when strong seismic activity and a rapid crustal deformation were observed. (2) The source of VLP is not small but elongates for ~4 km in the east-west direction at a south region of Inukura-yama, Ohmatsukura-yama, and Mitsuishi-yama. The depth is estimated to be 2 km. (3) Results of moment tensor inversion show that VLP is excited by a mutual deflation and inflation

process at the source region. Considering other geophysical evidences, such as seismic tomography and crustal deformation, we infer that mass and/or pressure transportation between two separated chambers excites the long-period waves, which is probably triggered by the opening of a narrow channel that connects the chambers. We present a simple source model based on one-dimensional flow dynamics and estimate the energy flow rate of the magmatic fluid to be 3 x 10^{12} J/s for the event on July 29, 1998.

Acknowledgments. We appreciate Eisuke Fujita who kindly helped our broadband seismic observation at GNB station. Careful reviews and comments of Associate Editor, Alan Linde, and two anonymous referees improved the manuscript and strengthened our source model. We used the database of hypocenters handled by the Japan Meteorological Agency (JMA) and the Science and Technology Agency, government of Japan. We are grateful to the following institutions that provided seismic waveform data for the hypocenter determination; National Research Institute for Earth Science and Disaster Prevention, Hokkaido University, Hirosaki University, Tohoku University, University of Tokyo, Nagoya University, Kyoto University, Kochi University, Kyushu University, Kagoshima University, Geological Survey of Japan, Tokyo Metropolitan Government, Shizuoka Prefectural Government, Hot Springs Research Institute of Kanagawa Prefecture, Japan Marine Science and Technology Center, Yokohama City Government and JMA. This research was partially supported by the Grant for Scientific Research from the Ministry of Education, Science and Culture, Japan (11640404).

References

Akaike, H., Information theory and an extension of the maximum likelihood principle, 2nd International Symposium on Information Theory, edited by B. N. Petrov, and F. Csaki, pp. 267-281, Akademiai Kiado, Budapest, 1973.

Bouchon, M., A simple method to calculate Green's functions for elastic layered media, *Bull. Seismol. Soc. Am.*, *71*, 959-971, 1981.

Chouet, B., Resonance of a fluid-driven crack: Radiation properties and implications for the source of long-period events and harmonitc tremor, *J. Geophys. Res* , *93*, 4375-4400, 1988.

Crosson, R. S., and D. A. Bame, A spherical source model for low frequency volcanic earthquakes, *J. Geophys. Res.*, *90*, 10,237-10,247, 1985.

Doi, Y., Volcanic activity of Mount Iwate since Johmon-era (in Japanese), *Chikyu Monthly*, *21*, 257-263, 1999.

Fujita, E., Y. Ida, and J. Oikawa, Eigen oscillation of a fluid sphere and source mechanism of harmonic volcanic tremor, *J. Volcanol. Geotherm. Res.*, *69*, 365-378, 1995.

Furumoto, M., T. Kunitomo, H. Inoue, and K. Yamaoka, Seismic image of the volcanic tremor source at Izu-Oshima volcano, Japan, in *Volcanic Seismology*, edited by P. Gasparini, R. Scarpa, and K. Aki, pp. 201-211, Springer-Verlag, New York, 1992.

Ide, S., M. Takeo, and Y. Yoshida, Source process of the 1995 Kobe earthquake; Determination of spatio-temporal slip distribution by Bayesian modeling, *Bull. Seismol. Soc Am* , *86*, 547-566, 1996.

Julian, B., Volcanic tremor: Nonlinear excitation by fluid flow, *J. Geophys Res.*, *99*, 11,859-11,877, 1994.

Kaneshima, S. et al., Mechanism of phreatic eruptions at Aso Volcano inferred from near-field broadband seismic observations, *Science*, *273*, 642-645, 1996.

Kennett, B. L. N. and N. J. Kerry, Seismic waves in a stratified half space, *Geophys. J R Astron. Soc.*, *57*, 557-583, 1979.

Nakagawa, M., Geology of Iwate volcanic group, northeastern Japan, *J. Mineral. Petrol. Econ. Geol.*, *82*, 132-150, 1987.

Nakagawa, M., and H. Togari, Mount Iwate in view of petrology: Recent magma system and characteristics of volcanic activity of Mount Iwate (in Japanese), *Chikyu Monthly*, *21*, 264-268, 1999.

Nakahara, H , T Nishimura, H. Sato, and M. Ohtake, Seismogram envelope inversion for the spatial distribution of high-frequency energy radiation from the earthquake fault: Application to the 1994 far east off Sanriku earthquake, Japan, *J Geophys. Res* , *103*, 855-867, 1998.

Nakahara, H., T. Nishimura, H. Sato, M. Ohtake, S. Kinoshita, S. Miura, S. Ueki, and H. Hamaguchi, Near field strong motions of the *M*6.1 earthquakes occurred at the northern part of Iwate Prefecture on September 3, 1998 (in Japanese), *Chikyu Monthly*, *21*, 322-326, 1999.

Neurberg, J., R. Luckett, M. Ripepe, and T. Braun, Highlights from a seismic broadband array on Stromboli volcano, *Geophys. Res. Lett.*, *21*, 749-752, 1994.

Nishimura, T., Source mechanisms of volcanic explosion earthquakes: Single force and implosive sources, *J. Volcanol Geotherm. Res.*, *86*, 97-106, 1998.

Nishimura, T., H. Nakahara, H. Sato, and M.Ohtake, Source process of the 1994 far east off Sanriku earthquake, Japan, as inferred from a broad-band seismogram, *Tohoku Geophys. J* , *34*, 121-134, 1996.

Ohminato, T., B.A. Chouet, P. Dawson, and S. Kedar, Waveform inversion of very long period impulsive signals associated with magmatic injection beneath Kilauea Volcano, Hawaii, *J. Geophys. Res.*, *103*, 23,839-23,862, 1998.

Rowe, C. A., R. C. Aster, P. R. Kyle, and J. W. Schlue, Broadband recording of Strombolian explosions and associated very long period seismic signals on Mount Erebus volcano, Ross Island, Antarctica, *Geophys. Res. Lett.*, *25*, 2297-2300, 1998.

Sacks, I. S., S. Suyehiro, D. W. Evertson, and Y. Yamagishi, Sacks-Everton strainmeter, it's installation in Japan and some preliminary results concerning strain step, *Pap. Meteorol. Geophys.*, *22*, 195-208, 1971.

Sato H., H. Takahashi, E. Yamamoto, N. Fukuo, M. Uehara, and Y. Terasawa, Development of the crustal tilt observation method using borehole-type tiltmeters (in Japanese with English abstract), *J. Seismol. Soc. Jpn.*, *33*, 343-368, 1980.

Sato, M., and H. Hamaguchi. Analyses of crustal deformation of Mount Iwate observed for a period from February to August 1998 (in Japanese), *Chikyu Monthly*, *21*, 312-317, 1999.

Tanaka, S., H. Nakamichi, H. Hamaguchi, and S. Ueki, The 1998 Seismic activity of Mount Iwate (in Japanese), *Chikyu Monthly*, *21*, 273-279, 1999a.

Tanaka, S., H. Nakamichi, T. Yamawaki, S. Ueki, and H. Hamaguchi, Three-dimensional seismic velocity structure of Iwate Volcano, Paper presented at 1999 Japan Earth and Planetary Science Joint Meeting, Tokyo, 1999b.

Tohoku University, Report of Coordinating Committee for Prediction of Volcanic Eruption, *73*, 16-24, Japan Meteorological Agency, 1999.

Ueki, S., Y. Morita, and H. Hamaguchi, On the volcanic tremor observed at Mount Iwate in Septebmer and October, 1995 (in Japanese), *Tohoku J. Natural Disaster Sci.*, *32*, 285-292, 1996.

Ueki, S., S. Miura, T. Sato, K. Tachibana, and H. Hamaguchi, The 1998 activity of crustal deformation of Mount Iwate detected by a dense GPS network observation (in Japanese), *Chikyu Monthly*, *21*, 296-302, 1999.

Ukawa, M., and M. Ohtake, A monochromatic earthquake suggesting deep-seated magmatic activity beneath the Izu-Ooshima Volcano, Japan, *J Geophys. Res* , *92*, 12,649-12,663, 1987.

H. Hamaguchi, H. Nakamichi, M. Sato, S. Tanaka, T. Nishimura and S. Ueki, Research Center for Prediction of Earthquakes and Volcanic Eruptions, Graduate School of Science, Tohoku University, Sendai 980-8578, Japan.(nishi@aob.geophys.tohoku.ac.jp)

T. Kobayashi, M. Ohtake, and H. Sato, Department of Geophysics, Graduate School of Science, Tohoku University, Sendai 980-8578, Japan.

(Received August 17, 1999; revised March 21, 2000;
accepted April 24, 2000.)